Load-Independent Power-Repeater Capacitive Power Transfer System With Multiple Constant Voltage Outputs

Ting Chen, Chenwen Cheng, Hong Cheng, Cong Wang, and Chunting Chris Mi, *Fellow, IEEE*

***Abstract*— In this article, a novel load-independent capacitive power transfer (CPT) system with multiple constant voltage (CV) outputs is proposed. The capacitive repeater unit is designed to enhance the power transfer capability, which contains four plates where two plates are used to receive power from its previous unit and the other two plates transfer power to the next unit. Electric coupling between the receiving and transmitting plates in the repeater unit can be eliminated by placing them perpendicularly and employing the split-inductor matching network. The load is connected with each capacitive repeater unit so that multiple loads can be powered simultaneously. Aluminum oxide ceramic is placed between the two adjacent units to enhance their electric coupling. The *L-LCL* network is adopted to compensate each capacitive repeater unit. Thus, CV outputs can be achieved for all loads, which ensure the independent operation of each load. The output voltages and efficiency are analyzed when considering the parasitic resistances. Finally, a three-load experimental setup is built to verify the effectiveness of the proposed system with an efficiency of 93.21%.**

***Index Terms*— Capacitive power transfer (CPT), constant voltage (CV) outputs, multiple loads, power-repeater.**

I. Introduction

WIRELESS power transfer (WPT) is emerging as a promising substitute for conventional cable charging, which demonstrates the attributes of safety, durability, and flexibility [1]. Recently, the multiload WPT system has been widely studied in battery charging [2], [3], light-emitting diode (LED) driving [4], reefer containers powering [5], online monitoring system powering [6], and gate drivers powering of insulated gate bipolar transistors (IGBTs) [7]. According to different power transfer mediums, either the inductive power transfer (IPT) or capacitive power transfer (CPT) [8] technology can be used.

In the multiload IPT system, Vu *et al.* [2] adopted the parallel connection of multiple one-transmitter and one-receiver IPT systems. However, the distance between every two transmitters–receivers should be large enough to avoid the undesired cross-coupling. In [3], multiple small receiving coils distributed in the same plane receive power from the same large transmitting coil simultaneously, but the cross-coupling issue remained unsolved. Lu *et al.* [9] and Xie *et al.* [10] proposed a WPT system with one transmitter and multiple power repeaters where multiple loads can be powered simultaneously. Nonetheless, the load outputs depend on each other, so that the independent load power control is difficult to implement in practical applications. Although the load-independent outputs are obtained in [10], the premise is that the cross-coupling effect between nonadjacent two coils is ignored. Furthermore, Cheng *et al.* [11] proposed a repeater unit formed by two perpendicular bipolar coils to eliminate cross-coupling. With a suitable compensation network design, multiple loads can be powered simultaneously and load-independent constant voltage (CV) outputs can be ensured.

Different from the above multiload IPT system, the energy of the multiload CPT system is transferred through the electric field, which avoids generating eddy current in the surrounding metal objects in the IPT system. Vu *et al.* [12] and Zhou *et al.* [13] adopted a parallel structure of multiple single-input and single-output CPT systems. Similar to the multiload IPT structure in [14], the cross-coupling issue was not considered. Su *et al.* [15] and Lillholm *et al.* [16] employed a large pair of transmitting plates and multiple pairs of small receiving plates to form the coupler. The receiving plates are in the same plane without considering the coupling capacitances between receivers. In [15], a variable inductor is designed to compensate for the coupling structure, and a T-*LCL* circuit is conducted to obtain constant current (CC) outputs. However, when one load suddenly varies, the rest load output currents will change accordingly. Thus, independent outputs for the multiload system were not achieved. In [16], independent power transfer to different receivers is achieved by ensuring a load-independent voltage across the transmitting

Manuscript received 28 September 2021; revised 6 February 2022 and 22 April 2022; accepted 13 May 2022. Date of publication 3 June 2022; date of current version 3 October 2022. This work was supported in part by the Fundamental Research Funds for the Central Universities under Grant 2242022R10123, in part by the Fujian Key Laboratory of New Energy Generation and Power Conversion under Grant KLIF-202101, in part by the National Engineering Laboratory of Energy-Saving Motor and Control Technique under Grant KFKT202209, in part by the National Natural Science Foundation of China under Grant 51977147, and in part by the Scholarship from the China Scholarship Council. *(Corresponding author: Chunting Chris Mi.)*

Ting Chen is with the State Key Laboratory of Reliability and Intelligence of Electrical Equipment, Hebei University of Technology, Tianjin 300130, China, and also with the School of Mechanical Electronic and Information Engineering, China University of Mining and Technology, Beijing 100083, China (e-mail: mia_tingchen@outlook.com).

Chenwen Cheng is with the School of Electrical Engineering, Southeast University, Nanjing 210096, China (e-mail: cheng.cwen@gmail.com).

Hong Cheng and Cong Wang are with the School of Mechanical Electronic and Information Engineering, China University of Mining and Technology, Beijing 100083, China (e-mail: chengh@cumtb.edu.cn; wangc@cumtb.edu.cn).

Chunting Chris Mi is with the Department of Electrical and Computer Engineering, San Diego State University, San Diego, CA 92182 USA (e-mail: mi@ieee.org).

Color versions of one or more figures in this article are available at https://doi.org/10.1109/JESTPE.2022.3180029.

Digital Object Identifier 10.1109/JESTPE.2022.3180029

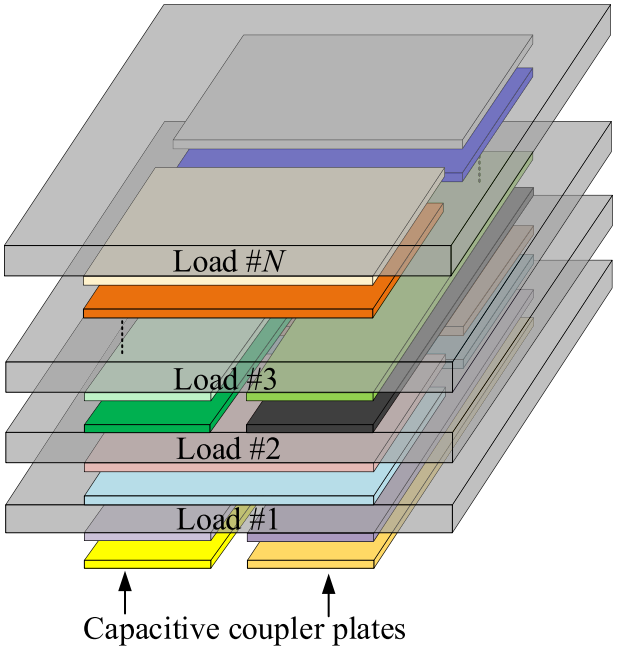

Fig. 1. Installation of the proposed power-repeater multiload CPT system.

plates through *LCCL* compensation circuit. Nevertheless, each receiver circuit must be resistive and the parasitic capacitance should be very little to be neglected. In order to suppress the cross-coupling between adjacent pairs of receiving plates, Kumar *et al.* [17] added tuning inductors that resonate with the parasitic capacitors between the two adjacent pairs of receiving plates. However, the parasitic capacitances are hardly measured accurately and the frequency has to be very high to reduce the size of the tuning inductors because of the small parasitic capacitance.

As a duality of multiload IPT system using repeater coils, Zhang *et al.* [18] proposed an electric field repeater in the CPT system where the repeater is solely used to extend the transmission distance of the CPT system and only one load can be powered. In order to power multiple loads simultaneously, Chen *et al.* [19] proposed a power-repeater CPT system with multiple load-independent current outputs, which can be utilized in the single-input and multiple-output stacked structure, as shown in Fig. 1. This structure is an extension of the domino IPT system into the CPT field. The CC can be obtained for all loads, which greatly simplified the load power control. However, the CV is preferred when powering online monitoring systems, miner light charging cabinets [13], or reefer containers [20]. In this case, an extra conversion circuit like the *LCL* circuit is required to be inserted before the load so that the CV source can be transformed to the CC source, which increases the system complexity and volume.

This article focuses on solving the problem that how to achieve power decoupling among multiple loads with CV outputs. Section II describes and models the proposed system. The way to achieve decoupling between capacitive repeater units is given in Section III. Section IV analyzes the output voltage and efficiency variations with the load resistance when considering the parasitic resistances. Finally, a three-load experimental prototype is established to validate the feasibility of the proposed power-repeater CPT system in Section V. The main contributions of this article are listed as follows.

1) The multiload CPT system with CV outputs adopting the decoupled capacitive coupler structure is proposed.
2) The split-inductor matching network is proposed to form the symmetrical compensation circuit, which can eliminate the influence of undesired stray couplings and simplify the system analysis.
3) Multiple loads can be powered simultaneously and independently with constant load voltages with the *L-LCL* compensation network, which avoids the load power coupling.

II. Modeling of Power-Repeater CPT System

A. System Modeling

Fig. 2 shows the structure of the proposed power-repeater multiload CPT system, which includes an inverter, one transmitting unit 0, one receiving unit N, and $N-1$ repeater unit 1–$N-1$. P_1 and P_2 form the transmitting plates in unit 0. $P_{4(N-1)+3}$ and $P_{4(N-1)+4}$ form the receiving plates in unit N. $P_{4(m-1)+3}$, $P_{4(m-1)+4}$, P_{4m+1} and P_{4m+2} are the four plates in repeater unit m ($m = 1, 2, \ldots, N-1$). The first two plates $P_{4(m-1)+3}$ and $P_{4(m-1)+4}$ are used to receive power from the previous unit, while P_{4m+1} and P_{4m+2} transfer power to the next unit. V_{dc} is the dc voltage of the inverter. In practical applications, an uncontrolled rectifier with a real dc load is connected at each output port. For facilitating the following analysis, the rectifier load is modeled as an ac load resistance $R_{L,m}$ ($m = 1, 2, \ldots, N$). External capacitors $C_{\mathrm{ex1},m}$ ($m = 1, 2, \ldots, N$) are connected in parallel with $P_{4(m-1)+1}$ and $P_{4(m-1)+2}$. External capacitors $C_{\mathrm{ex2},m}$ ($m = 1, 2, \ldots, N$) are connected in parallel with $P_{4(m-1)+3}$ and $P_{4(m-1)+4}$. $C_{f,m}$ ($m = 1, 2, \ldots, N$) is the compensation capacitors. L_{f,m_1}, L_{f,m_2}, L_{1,m_1}, L_{1,m_2}, L_{2,m_1} and L_{2,m_2} ($m = 1, 2, \ldots, N$) are the compensation inductors with the following relationship:

$$L_{f,m\_1} = L_{f,m\_2}, \quad L_{1,m\_1} = L_{1,m\_2}, \quad L_{2,m\_1} = L_{2,m\_2}. \quad (1)$$

Thus, a symmetrical compensation network can be formed, whose functionality will be analyzed in Section III. V_{in} and I_{in} are the inverter output voltage and current, respectively. Due to the low-pass filter characteristics of the compensation network, the fundamental harmonics approximation (FHA) method can be used to analyze the proposed power-repeater system [21]. When the inverter operates in a complementary manner, the amplitude of the fundamental output voltage V_{in1} can be expressed as

$$V_{\mathrm{in1}} = 2\sqrt{2}V_{\mathrm{dc}}/\pi. \quad (2)$$

The proposed system in Fig. 2 can be regarded as the cascaded circuit of N transmitter–receiver pairs. Since the currents flowing through the forward path and the return path are the same as analyzed in Section III-C, the compensation inductor in the forward path and the compensation inductor in the return path can be combined as one inductor. For example, L_{f,m_1} in the forward path and L_{f,m_2} in the return path can

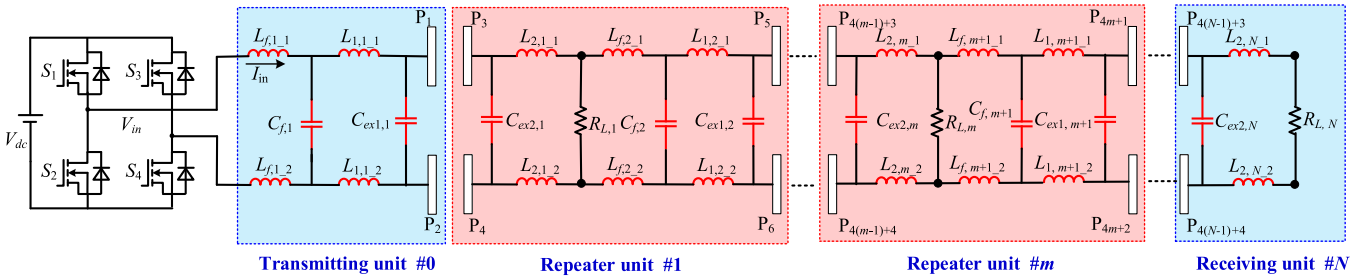

Fig. 2. Structure of the proposed power-repeater multiload CPT system.

be combined as $L_{f,m}$. Then, the following expression can be met:

$$L_{f,m} = L_{f,m\_1} + L_{f,m\_2}, \quad L_{1,m} = L_{1,m\_1} + L_{1,m\_2}$$
$$L_{2,m} = L_{2,m\_1} + L_{2,m\_2}. \tag{3}$$

Therewithal, the capacitive plates are modeled as the equivalent Π circuit. The proposed system in Fig. 2 can be redrawn in Fig. 3. $\boldsymbol{V}_{RL,0}$ is exactly V_{in1}. $C_{1,m}$ and $C_{2,m}$ $(m = 1, 2, \ldots, N)$ are the equivalent self-capacitance and can be expressed as follows [21]:

$$C_{1,m} = C_{\text{in1},m} + C_{\text{ex1},m}, \quad C_{2,m} = C_{\text{in2},m} + C_{\text{ex2},m} \tag{4}$$

where $C_{\text{in1},m}$ and $C_{\text{in2},m}$ are the internal self-capacitances. $C_{M,m}$ $(m = 1, 2, \ldots, N)$ is the mutual capacitances between $P_{4(m-1)+1}$, $P_{4(m-1)+2}$, $P_{4(m-1)+3}$, and $P_{4(m-1)+4}$. Their corresponding coupling coefficient $k_{c,m}$ $(m = 1, 2, \ldots, N)$ can be expressed as

$$k_{c,m} = C_{M,m}/\sqrt{C_{1,m}C_{2,m}}. \tag{5}$$

It is noteworthy that the coupling coefficient in each repeater unit is zero with a proper capacitive coupler design as discussed in Section III.

B. CV Outputs

In this section, all parasitic resistances are neglected first to simplify the analysis. The effect of parasitic resistances on system performances will be analyzed in Section IV. The currents flowing through $L_{f,m}$, $C_{f,m}$, $L_{1,m}$, $C_{1,m} - C_{M,m}$, $C_{M,m}$, $C_{2,m} - C_{M,m}$, $L_{2,m}$, and $R_{L,m}$ $(m = 1, 2, \ldots, N)$ are represented by $\boldsymbol{I}_{Lf,m}$, $\boldsymbol{I}_{Cf,m}$, $\boldsymbol{I}_{L1,m}$, $\boldsymbol{I}_{C1,m}$, $\boldsymbol{I}_{CM,m}$, $\boldsymbol{I}_{C2,m}$, $\boldsymbol{I}_{L2,m}$, and $\boldsymbol{I}_{RL,m}$ $(m = 1, 2, \ldots, N)$, respectively. The directions of these currents and voltages are defined in Fig. 3. $C_{f,m}$ is designed to be resonated with $L_{f,m}$, i.e.,

$$\omega_0^2 = 1/\left(L_{f,m}C_{f,m}\right) \tag{6}$$

thereby a CC output $\boldsymbol{I}_{L1,m}$, as shown in Fig. 4, is obtained according to [21] and can be expressed as

$$\mathbf{I}_{L1,m} = \mathbf{V}_{RL,m-1}/\left(j\omega_0 L_{f,m}\right) \tag{7}$$

where ω_0 is the operational angular frequency of the system. According to Thevenin's theorem, the circuit can be equivalently transformed into a voltage source and an internal resistance in series. In order to obtain a CV output, the internal impedance should be zero. When calculating the internal resistance, the current source $\boldsymbol{I}_{L1,m}$ is regarded as open. If $L_{2,m}$ is designed to be resonated with the equivalent capacitance $C_{\text{sec},m}$ seen from the secondary side, i.e.,

$$\omega_0^2 = 1/\left(L_{2,m}C_{\text{sec},m}\right) = 1/\left(L_{2,m}\left(\left(C_{2,m}C_{1,m} - C_{M,m}^2\right)/C_{1,m}\right)\right) \tag{8}$$

the internal impedance is a series resonant circuit whose equivalent impedance is zero. In this case, the Thevenin equivalent circuit is a voltage source $\boldsymbol{V}_{RL,m}$, as shown in Fig. 4, which means the voltage across $R_{L,m}$ is $\boldsymbol{V}_{RL,m}$ and can be derived as

$$\begin{aligned}\mathbf{V}_{RL,m} &= \frac{C_{M,m}}{j\omega_0\left(C_{1,m}C_{2,m} - C_{M,m}^2\right)}\mathbf{I}_{L1,m} \\ &= \frac{-\mathbf{V}_{RL,m-1}C_{M,m}}{\omega_0^2 L_{f,m}\left(C_{1,m}C_{2,m} - C_{M,m}^2\right)}\end{aligned} \tag{9}$$

where $\boldsymbol{V}_{RL,0}$ is exactly $\boldsymbol{V}_{\text{in1}}$. To achieve equal CV outputs, (10) should be satisfied. It can be identified from (9) that the phase angle difference between any two adjacent output voltages is 180°

$$C_{M,m}/\left(\omega_0^2 L_{f,m}\cdot\left(C_{1,m}C_{2,m} - C_{M,m}^2\right)\right) = 1. \tag{10}$$

The impedance of the subsequent circuit after $R_{L,m}$ is defined as $Z_{\text{in},m+1}$. The load impedance $Z_{R,m}$ of the mth $(m = 1, 2, \ldots, N-1)$ transmitter–receiver pair is the parallel-connection circuit of $R_{L,m}$ and $Z_{\text{in},m+1}$. The load impedance $Z_{R,N}$ of the last transmitter–receiver pair is $R_{L,N}$. They can be expressed as

$$Z_{R,m} = \begin{cases} R_{L,m}Z_{\text{in},m+1}/\left(R_{L,m} + Z_{\text{in},m+1}\right), \\ \qquad m = 1, 2, \ldots, N-1 \\ R_{L,N}, \\ \qquad m = N. \end{cases} \tag{11}$$

Then, the input impedance $Z_{\text{in},m}$ $(m = 1, 2, \ldots, N)$ of each transmitter–receiver pair can be calculated as

$$Z_{\text{in},m} = 1/\left[\frac{Z_{L2,m}^2}{Z_{Lf,m}^2 Z_{R,m}} + j\left(\frac{Z_{L1,m} - Z_{L2,m}}{Z_{Lf,m}^2} - \frac{1}{Z_{Lf,m}}\right)\right] \tag{12}$$

where $Z_{Lf,m} = \omega_0 L_{f,m}$, $Z_{L1,m} = \omega_0 L_{1,m}$, and $Z_{L2,m} = \omega_0 L_{2,m}$ are the impedance of $L_{f,m}$, $L_{1,m}$, and $L_{2,m}$, respectively. For the sake of eliminating reactive power in the circuit, the input zero phase angle (ZPA) should be achieved. Since $Z_{R,N}$ of the last transmitter–receiver pair is resistive, as long as $Z_{L1,m} = Z_{L2,m} + Z_{Lf,m}$ $(m = 1, 2, \ldots, N)$ is met accordingly,

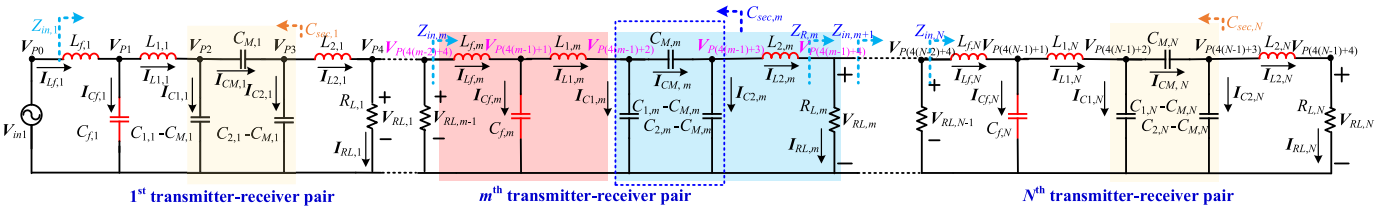

Fig. 3. Equivalent Π model of the mth transmitter–receiver pair using the FHA modeling method ($m = 1, 2, \ldots, N$).

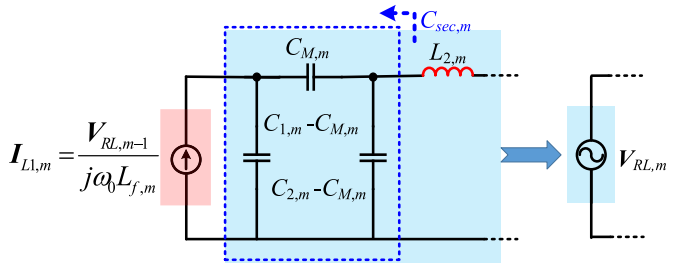

Fig. 4. Equivalent circuit model of the mth transmitter–receiver pair.

$Z_{\text{in},m}$ is also resistive. Thus, the relationship of compensation inductances in the proposed topology should satisfy

$$L_{1,m} = L_{2,m} + L_{f,m}. \tag{13}$$

As can be seen from (22)–(13), once $C_{M,m}$, $C_{1,m}$, and $C_{2,m}$ are determined beforehand, other compensation parameters can be derived accordingly and the amplitudes of all load output voltage $V_{RL,m}$ are identical. Meanwhile, $L_{2,m}$ can be derived from (8). $L_{f,m}$ can be derived from (10). Then, $C_{f,m}$ can be derived from (22), and $L_{1,m}$ can be derived from (13). If the mutual capacitances and equivalent self-capacitances met $C_{M,1} = C_{M,2} = \cdots C_{M,N} = C_M$, $C_{1,1} = C_{1,2} = \cdots C_{1,N} = C_1$, and $C_{2,1} = \cdots C_{2,2} = C_{2,N} = C_2$, the coupling coefficients, corresponding inductances and capacitances in all repeater units would be equal, i.e., $k_{c,1} = k_{c,2} = k_{c,N} = k$, $L_{f,1} = L_{f,2} = L_{f,N} = L_f$, $L_{1,1} = L_{1,2} = L_{1,N} = L_1$, $L_{2,1} = L_{2,2} = L_{2,N} = L_2$, $C_{f,1} = C_{f,2} = \cdots C_{f,N} = C_f$. It should be noted that no matter how far away each repeater unit is from the transmitting unit, the proposed system can achieve the same output voltage. Therefore, under the premise that all load resistances are the same, i.e., $R_{L,1} = R_{L,2} = \cdots = R_{L,N} = R_L$, all loads can receive the same amount of power.

III. Capacitive Coupler Design

A. Coupler Decoupling Mechanism

In a simplest CPT system formed by four plates (P_1–P_4), the simplified equivalent Π model of the coupler is obtained on the premise that the model of six coupling capacitors is modeled as a two-port network with v_{P1P3} and v_{P3P4} as the input variables, and $i_1(-i_2)$ and $i_3(-i_4)$ as the output variables [21], as shown in Fig. 5(a) and (b). It means $i_1 = -i_2$ and $i_3 = -i_4$ should be both satisfied. The mutual capacitance C_{mutual} can be expressed as [21]

$$C_{\text{mutual}} = \frac{C_{2\_4} \cdot C_{1\_3} - C_{1\_4} \cdot C_{2\_3}}{C_{1\_3} + C_{1\_4} + C_{2\_3} + C_{2\_4}}. \tag{14}$$

If P_1 and P_2 are placed perpendicular to P_3 and P_4 with the same facing areas, as shown in Fig. 5(c),

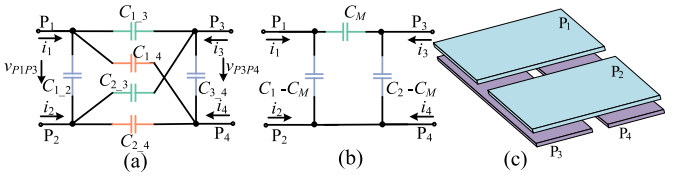

Fig. 5. Equivalent circuit model of the capacitive coupler. (a) Circuit model of the coupling capacitors. (b) Simplified equivalent Π model of coupling capacitors. (c) Perpendicular four plates.

$C_{2\_4} = C_{1\_3} = C_{1\_4} = C_{2\_3}$ can be obtained because of symmetry when all plates have the same size. In this case, $C_{\text{mutual}} = 0$, which indicates that the capacitive decoupling is achieved. To sum up, two conditions should be met to achieve decoupling. The first one is that the equivalent circuit model of the capacitive coupler should be a two-port network. The other one is to adopt the perpendicular coupler structure.

B. Capacitive Power-Repeater Coupler

The CV outputs of the aforementioned analysis in Section II are based on the assumption that the capacitive coupling within each repeater unit is eliminated. To achieve this goal, according to the above analysis in part A, the capacitive power-repeater coupler of the multiload CPT system is presented in Fig. 6. Aluminum oxide ceramics are embedded in each transmitter–receiver pair formed by four plates ($P_{4(m-1)+1}$, $P_{4(m-1)+2}$, $P_{4(m-1)+3}$ and $P_{4(m-1)+4}$, $m = 1, 2, \ldots, N$) to increase the coupling capacitance. In each capacitive repeater formed by four plates ($P_{4(m-1)+3}$, $P_{4(m-1)+4}$, P_{4m+1} and P_{4m+2}, $m = 1, 2, \ldots, N-1$), two transmitting plates are placed perpendicular to the two receiving plates. The length and width of the plates are l_1 and l_2, respectively. The plate separation on the same side is d_1, which satisfies $d_1 = l_1 - 2l_2$. The thickness of the plates is d_2. The ceramic-gap distance between adjacent repeater units is d_3. The air-gap distance in each repeater is d_4. The coupling capacitance between plate P_i and P_j ($i, j = 1, 2, \ldots, 4(N-1)+4$, $i \neq j$) is defined as C_{i_j}.

The finite element analysis (FEA) is employed to simulate coupling capacitances and design the dimensions of the repeater. The length l_1 and the thickness d_2 of the plates are 150 and 2 mm, respectively. Fig. 7(a) shows mutual capacitance variations with various plate separation distances d_1 under the premise of different ceramic-gap d_3. It can be seen that the mutual capacitance decreases with the growing plate separation distance d_1. A smaller ceramic-gap d_3 will lead to higher mutual capacitance. Thus, the plate separation distance d_1 and the ceramic-gap d_3 should be small enough to achieve larger coupling. When d_1 is selected as 20 mm and d_3

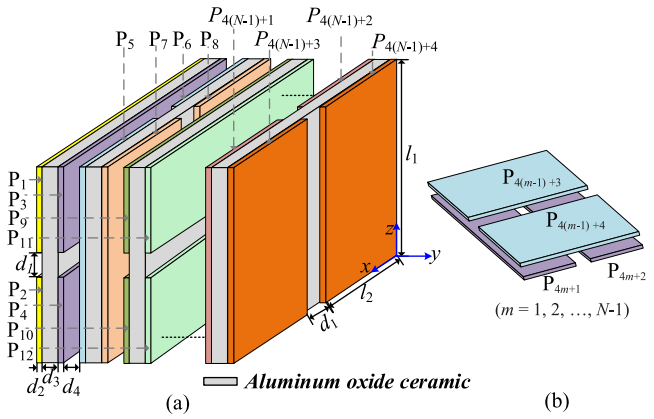

Fig. 6. Power-repeater coupler of the multiload CPT system. (a) Whole repeater coupler. (b) One repeater coupler.

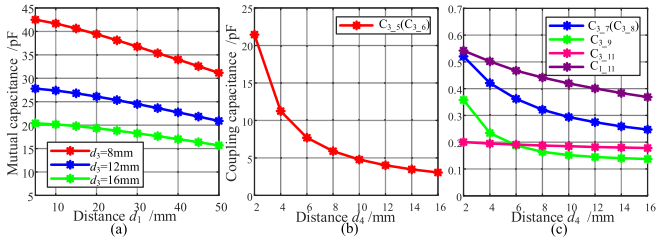

Fig. 7. (a) Mutual capacitance variations with different plate separation distance d_1 and different ceramic-gap d_3. The coupling capacitance of two power-repeater system variations with different air-gap d_4 under the premise of $d_1 = 20$ mm and $d_3 = 8$ mm with two (b) adjacent plates and (c) nonadjacent plates.

TABLE I
DIMENSIONS OF THE POWER-REPEATER COUPLER

l_1	150mm	d_1	20mm	d_3	8mm
l_2	65mm	d_2	2mm	d_4	8mm

is selected as 8 mm, the mutual capacitance $C_{M,1}$ is around 39 pF. Fig. 7(b) and (c) shows the coupling capacitance variations with different air-gap d_4 in a two-power-repeater system. The coupling capacitance between two plates with facing area is much larger than the capacitance between the other two plates, so only C_{3_5}, C_{3_6}, C_{3_7}, C_{3_8}, C_{3_9}, C_{3_11}, and C_{1_11} are presented for comparison. It can be seen that the coupling capacitance of two adjacent plates is much larger than that of two nonadjacent plates when d_4 varies from 2 to 16 mm. Thus, the coupling capacitances between any two nonadjacent plates can be neglected. Considering system volume, d_4 is also selected as 8 mm. The dimensions of the power-repeater coupler are summarized in Table I.

According to the above simulation results, it can be derived that only the coupling capacitances between four adjacent plates should be considered. The coupling capacitances between the other plates are very small so that they can be ignored to simplify the analysis. Hence, the model of coupling capacitors of the proposed power-repeater multiload CPT system is shown in Fig. 8. The coupling capacitances in repeater unit m are defined as part A_m. The compensation circuit and load in repeater unit m are defined as part B_m. The coupling capacitances in the mth transmitter–receiver pair are defined as part D_m. The voltage between plate P_i and P_j is defined as v_{PiPj}. According to the perpendicular structure of the repeater unit m in Fig. 6, (15) can be obtained because the relative areas of the four plates are equal

$$C_{4(m-1)+3\_4m+1} = C_{4(m-1)+3\_4m+2} = C_{4(m-1)+4\_4m+1} = C_{4(m-1)+4\_4m+2}. \tag{15}$$

C. Two-Port Network Analysis and Power-Repeater Coupler Modeling

Based on the above perpendicular power-repeater structure, if Parts A_m and B_m in unit m ($m = 1, 2, \ldots, N$) in Fig. 8 are both two-port networks, the load power decoupling can be achieved. However, due to the existence of compensation network and load resistance in repeater units, it remains unclear whether Parts A_m and B_m are two-port networks. The following context will prove that Parts A_m and B_m are two-port networks when the compensation networks are symmetrical, which means a split matching network, as shown in Fig. 2, should be employed.

Since all repeater units have the same structure, repeater unit 1 is taken as an example to prove the above conclusion. The voltages between P_3 and P_4 can be modeled as two sinusoidal voltage sources with the same magnitude but 180° phase difference. So do the voltages between P_5 and P_6. The voltages across P_3–P_6 are defined as v_{P3}–v_{P6}, respectively, and they can be expressed as

$$\begin{cases} v_{P3} = 0.5 \cdot V_{P3P4} \sin(\omega_0 t + \varphi_1), \\ v_{P4} = 0.5 \cdot V_{P3P4} \sin\left(\omega_0 t + \varphi_1 + 180^\circ\right) \\ v_{P5} = 0.5 \cdot V_{P5P6} \sin(\omega_0 t + \varphi_2), \\ v_{P6} = 0.5 \cdot V_{P5P6} \sin\left(\omega_0 t + \varphi_2 + 180^\circ\right) \end{cases} \tag{16}$$

where φ_1 is the initial phase angle of v_{P3} and v_{P4}, φ_2 is the initial phase angle of v_{P5} and v_{P6}.

Fig. 9 shows the equivalent circuits when only one voltage source is applied, while others are short-circuited. The voltages and currents in the repeater unit can be derived by using the superposition theorem. The definitions and directions of currents flowing through C_{3_5}, C_{3_6}, C_{4_5}, C_{4_6}, $L_{2,1\_1}$, $L_{2,1\_2}$, $L_{1,2\_1}$, and $L_{1,2\_2}$ are defined in Figs. 8 and 9. In the repeater unit, the compensation components located at the symmetrical position have the same value according to (1) and (15). Since the magnitude of v_{p3} and v_{p4} is equal and their phase angle difference is 180°, the currents flowing through repeater unit 1 located in the symmetrical position have the same amplitude and opposite directions, i.e., $i_{C35\_1} = -i_{C46\_2}$, $i_{C36\_1} = -i_{C45\_2}$, $i_{C46\_1} = -i_{C35\_2}$, $i_{C45\_1} = -i_{C36\_2}$, $i_{x1\_1} = -i_{y1\_2}$, $i_{y1\_1} = -i_{x1\_2}$, $i_{x2\_1} = -i_{y2\_2}$. Similarly, $i_{C35\_3} = -i_{C46\_4}$, $i_{C45\_3} = -i_{C36\_4}$, $i_{C46\_3} = -i_{C35\_4}$, $i_{C36\_3} = -i_{C45\_4}$, $i_{x1\_3} = -i_{y1\_4}$, $i_{y1\_3} = -i_{x1\_4}$, and $i_{x2\_3} = -i_{y2\_4}$ can be derived because the magnitudes of v_{p5} and v_{p6} are equal and their phase angle difference is 180°. Besides, the currents flowing through all circuit components of repeater unit 1 are equal to the sum of currents when four independent source works separately. Thus, the following equation can be obtained:

$$\begin{cases} i_{C35} + i_{C36} = -(i_{C45} + i_{C46}), \quad i_{x1} = -i_{y1} \\ i_{C35} + i_{C45} = -(i_{C36} + i_{C46}), \quad i_{x2} = -i_{y2}. \end{cases} \tag{17}$$

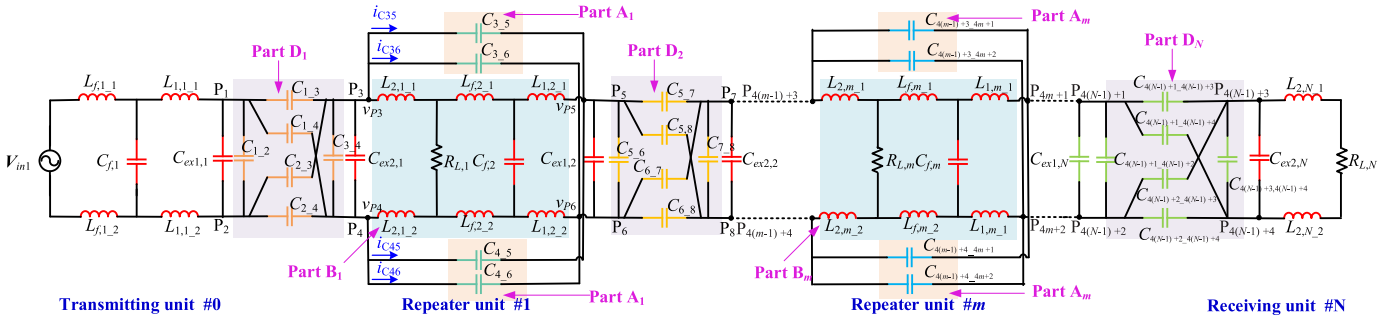

Fig. 8. Model of coupling capacitors of the proposed power-repeater multiload CPT system.

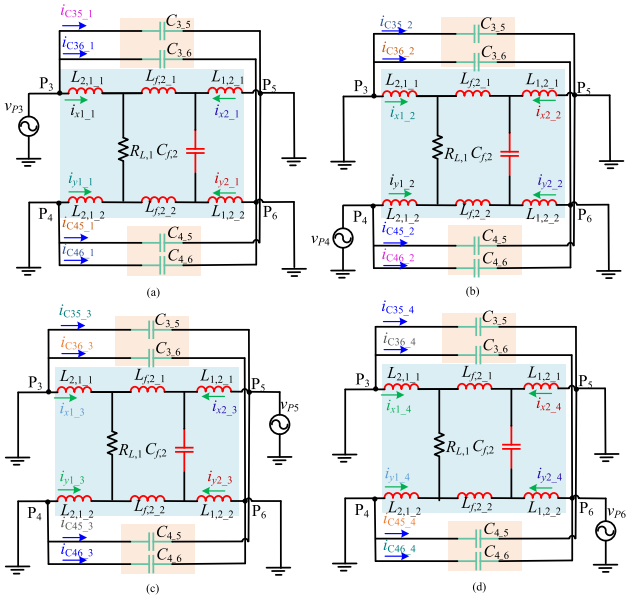

Fig. 9. Equivalent model of repeater unit 1 with only (a) v_{P3} works and other power supplies are short-circuited, (b) v_{P4} works and other power supplies are short-circuited, (c) v_{P5} works and other power supplies are short-circuited, and (d) v_{P6} works and other power supplies are short-circuited.

It can be identified from (17) that Parts A_1 and B_1 are two-port networks. Thus, the mutual capacitance $C_{Mr,1}$ can be derived as follows by adopting the method in [21]:

$$C_{Mr,1} = \left(C_{4\_6} \cdot C_{3\_5} - C_{4\_5} \cdot C_{3\_6}\right) / \left(C_{3\_5} + C_{4\_5} + C_{3\_6} + C_{4\_6}\right). \quad (18)$$

According to (15), $C_{3\_5} = C_{3\_6} = C_{4\_5} = C_{4\_6}$ can be obtained when $m = 1$. Substituting this equation into (18), it can be obtained that $C_{Mr,1}$ is zero. Thus, P_3–P_6 in repeater unit 1 are decoupled and the capacitive coupler formed by them is a two-port network. This conclusion can be generalized to other repeater units. Besides, Part D_m ($m = 1, 2, \ldots, N$) are all two-port networks because of no other branches in them. Therefore, the existing modeling and calculation method of the mutual capacitance and self-capacitance of single-input single-output coupling interfaces in [21] can be applied to this power-repeater multiload CPT system. Considering the equivalent circuit model of the four-plate coupler in [21], the internal self-capacitance $C_{\text{in1},1}$ and $C_{\text{in2},N}$ are the self-capacitance of Parts D_1 and D_N, respectively. The internal self-capacitance $C_{\text{in2},m}$ ($m = 1, 2, \ldots, N-1$) and $C_{\text{in1},m}$ ($m = 2, 3, \ldots, N$) are the sum of the self-capacitances of two adjacent units, respectively. All self-capacitances can be calculated as (19). The mutual capacitance $C_{M,m}$ ($m = 1, 2, \ldots, N$) can be calculated as (20).

TABLE II
CIRCUIT PARAMETERS OF THE PROPOSED SYSTEM

Parameter	Value	Parameter	Value
N	3	$L_{f,1\_1}$, $L_{f,2\_1}$, $L_{f,3\_1}$, $L_{f,1\_2}$, $L_{f,2\_2}$, $L_{f,3\_2}$	3.3μH
V_{dc}	35V	$L_{1,2\_1}$, $L_{1,3\_1}$, $L_{1,2\_2}$, $L_{1,3\_2}$	25.3μH
$k_{c,1}$, $k_{c,2}$, $k_{c,3}$	0.15	$L_{2,1\_1}$, $L_{2,2\_1}$, $L_{2,3\_1}$, $L_{2,1\_2}$, $L_{2,2\_2}$, $L_{2,3\_2}$	22μH
$C_{f,1}$~ $C_{f,3}$	1.71nF	$L_{1,1\_1}$, $L_{1,1\_2}$	22.3μH
$C_{ex1,1}$, $C_{ex2,3}$	219pF	$C_{ex2,1}$, $C_{ex1,2}$, $C_{ex2,2}$, $C_{ex1,3}$	214pF

It should be noted that adopting the split-inductor matching network is the premise that Parts A_m and B_m of repeater coupler m are the two-port networks. If the split-inductor matching network is not employed, (18) is not satisfied anymore so that the proposed power-repeater system is not decoupled. This can be verified by LTspice simulations. Fig. 10 shows the simulation results of the load voltages of a three-load power-repeater CPT system with the experimental parameters in Table II when split-inductor symmetrical matching network is adopted or not. It can be seen that when the split-inductor matching networks are employed, the three load output voltages are identical. However, without the split-inductor matching network, the three load outputs have an additional voltage drop. Besides, the farther the load is from the first repeater unit, the greater the load output voltage drops (19), as shown at the bottom of the next page.

IV. POWER TRANSFER CAPABILITY

In a practical system, the parasitic resistances of the compensation network are inevitable, whose influence needs to be analyzed. Without losing generality, it is assumed that the quality factors Q of all components are identical to simplify the analysis. The parasitic resistances and the admittance can be expressed as (21), as shown at the bottom of the next page, where $r_{Lf,m}$, $r_{L1,m}$, $r_{L2,m}$, $r_{C1,m}$, $r_{C2,m}$, $r_{Cf,m}$, and $r_{CM,m}$ represent the parasitic resistances of $L_{f,m}$, $L_{1,m}$, $L_{2,m}$, $C_{1,m}-C_{M,m}$, $C_{2,m}-C_{M,m}$, $C_{f,m}$, and $C_{M,m}$, respectively. $Y_{Lf,m}$, $Y_{L1,m}$, $Y_{L2,m}$, $Y_{C1,m}$, $Y_{C2,m}$, $Y_{Cf,m}$, $Y_{CM,m}$, and $Y_{RL,m}$ represent the admittance of $L_{f,m}$, $L_{1,m}$, $L_{2,m}$, $C_{1,m}-C_{M,m}$, $C_{2,m}-C_{M,m}$, $C_{f,m}$, $C_{M,m}$, and $R_{L,m}$, respectively.

A. Output Voltages

In order to facilitate the system analysis about the influence of parasitic resistances on the load output voltages, the

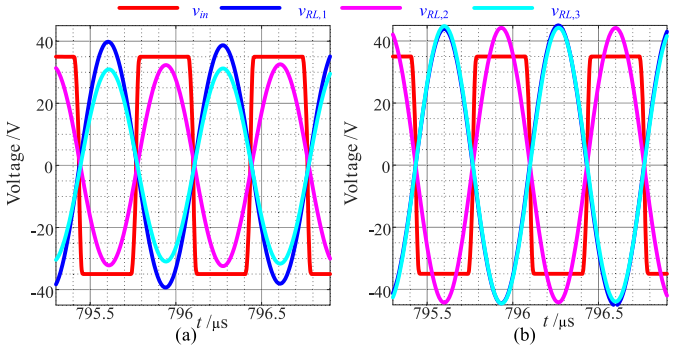

Fig. 10. Three load output voltages (a) without the split-inductor matching network and (b) with the split-inductor matching network.

node voltage method is adopted according to Fig. 3 and the following equation can be obtained:

$$\begin{bmatrix} \boldsymbol{G}_1 & \boldsymbol{A}_1 & \mathbf{O} & \mathbf{O} & \cdots & \mathbf{O} & \mathbf{O} \\ \boldsymbol{B}_2 & \boldsymbol{G}_2 & \mathbf{A}_2 & \mathbf{O} & \cdots & \mathbf{O} & \mathbf{O} \\ \mathbf{O} & \mathbf{B}_3 & \mathbf{G}_3 & \mathbf{O} & \cdots & \mathbf{O} & \mathbf{O} \\ \cdots & \cdots & \cdots & \cdots & \cdots & \cdots & \\ \mathbf{O} & \mathbf{O} & \mathbf{O} & \mathbf{O} & \cdots & \mathbf{B}_N & \mathbf{G}_N \end{bmatrix} \begin{bmatrix} \boldsymbol{V}_{p1} \\ \mathbf{V}_{p2} \\ \mathbf{V}_{p3} \\ \cdots \\ \mathbf{V}_{pN} \end{bmatrix} = \begin{bmatrix} \mathbf{I} \\ \mathbf{o} \\ \mathbf{o} \\ \cdots \\ \mathbf{o} \end{bmatrix} \quad (22)$$

where matrices $\boldsymbol{G}_m$ $(m = 1, 2, \ldots, N)$ can be expressed as (23). $\boldsymbol{A}_{\mathbf{m}} = [0\ 0\ 0\ 0;\ 0\ 0\ 0\ 0;\ 0\ 0\ 0\ 0;\ -Y_{Lf,m+1}\ 0\ 0\ 0]$. $\boldsymbol{B}_{\mathbf{m}} = [0\ 0\ 0\ -Y_{Lf,m};\ 0\ 0\ 0\ 0;\ 0\ 0\ 0\ 0;\ 0\ 0\ 0\ 0]$. $\boldsymbol{I} = [-Y_{Lf,1}\ \boldsymbol{V}_{\mathrm{in1}}\ 0\ 0\ 0]$. $\boldsymbol{O}$ represents 4×4 zero matrix. $\boldsymbol{o}$ represents 4×1 zero matrix. $\boldsymbol{V}_{\mathrm{pm}} = [\ \boldsymbol{V}_{P(4(m-1)+1)}\ \boldsymbol{V}_{P(4(m-1)+2)}\ \boldsymbol{V}_{P(4(m-1)+3)}\ \boldsymbol{V}_{P(4(m-1)+4)}]$, where $\boldsymbol{V}_{P(4(m-1)+1)}$, $\boldsymbol{V}_{P(4(m-1)+2)}$, $\boldsymbol{V}_{P(4(m-1)+3)}$, and $\boldsymbol{V}_{P(4(m-1)+4)}$ $(m = 1, 2, \ldots, N)$ denote the node voltages in the mth transmitter–receiver pair (23), as shown at the bottom of the next page.

By solving (22), the node voltages $\boldsymbol{V}_{P1}$, $\boldsymbol{V}_{P2}, \ldots,$ $\boldsymbol{V}_{P(4(N-1)+4)}$ can be derived and the load output voltage $\boldsymbol{V}_{RL,m}$ $(m = 1, 2, \ldots, N)$ is equal to $\boldsymbol{V}_{P(4(m-1)+4)}$. To facilitate comparisons, the base voltage V_b is defined as the fundamental component of the inverter output voltage V_{in1}. According to (9), the base load resistance R_b can be derived by dividing $\boldsymbol{V}_{RL,m}$ by the input current $\boldsymbol{I}_{L1,m}$ and can be expressed as

$$R_b = \boldsymbol{V}_{RL,m}/\boldsymbol{I}_{L1,m} = 1/\left(\omega_0 C_{M,m}(1/k_{c,m}^2 - 1)\right). \quad (24)$$

With the parameters in Table II, Fig. 11(a) shows the normalized load voltage variations versus the normalized load resistance. It can be seen that the load voltage decreases gradually as the load resistance increases. Moreover, the load voltage decreases faster if the unit is farther from transmitting unit 0. As the normalized load resistance increases, the voltage attenuation becomes larger. Fig. 11(b) shows load voltage variations flowing through the third load with different coupling coefficients and quality factors when there are three loads and the normalized load resistance is 0.6. It can be seen that a larger quality factor Q leads to a higher load voltage. Besides, the normalized load voltage will increase with the increase of the coupling coefficient. Thus, the higher quality factor and higher coupling coefficient are beneficial from the perspective of CV outputs.

Fig. 12 shows the mutual capacitances and self-capacitances variations with the four plates in repeater unit 1 under x-axis misalignment conditions. This figure indicates that the maximum mutual capacitance and self-capacitances variations

$$\begin{cases} C_{\mathrm{in}1,1} = C_{1\_2} + (C_{1\_3} + C_{1\_4}) \cdot (C_{2\_3} + C_{2\_4})/\left(C_{1\_3} + C_{1\_4} + C_{2\_3} + C_{2\_4}\right) \\ C_{\mathrm{in}2,m} = C_{4(m-1)+3\_4(m-1)+4} + \dfrac{\left(C_{4(m-1)+1\_4(m-1)+3} + C_{4(m-1)+2\_4(m-1)+3}\right) \cdot \left(C_{4(m-1)+1\_4(m-1)+4} + C_{4(m-1)+2\_4(m-1)+4}\right)}{\left(\begin{array}{l} C_{4(m-1)+1\_4(m-1)+3} + C_{4(m-1)+1\_4(m-1)+4} \\ + C_{4(m-1)+2\_4(m-1)+3} + C_{4(m-1)+2\_4(m-1)+4} \end{array}\right)} + \dfrac{\left(C_{4(m-1)+3\_4m+1} + C_{4(m-1)+3\_4m+2}\right) \cdot \left(C_{4(m-1)+4\_4m+1} + C_{4(m-1)+4\_4m+2}\right)}{\left(\begin{array}{l} C_{4(m-1)+3\_4m+1} + C_{4(m-1)+4\_4m+1} \\ + C_{4(m-1)+3\_4m+2} + C_{4(m-1)+4\_4m+2} \end{array}\right)}, \quad m = 1, 2, \ldots, N-1 \\ C_{\mathrm{in}1,m} = C_{4(m-1)+1\_4(m-1)+2} + \dfrac{\left(C_{4(m-1)+1\_4(m-1)+3} + C_{4(m-1)+1\_4(m-1)+4}\right) \cdot \left(C_{4(m-1)+2\_4(m-1)+3} + C_{4(m-1)+2\_4(m-1)+4}\right)}{\left(\begin{array}{l} C_{4(m-1)+1\_4(m-1)+3} + C_{4(m-1)+1\_4(m-1)+4} \\ + C_{4(m-1)+2\_4(m-1)+3} + C_{4(m-1)+2\_4(m-1)+4} \end{array}\right)} + \dfrac{\left(C_{4(m-2)+3\_4(m-1)+1} + C_{4(m-2)+4\_4(m-1)+1}\right) \cdot \left(C_{4(m-2)+3\_4(m-1)+2} + C_{4(m-2)+4\_4(m-1)+2}\right)}{\left(\begin{array}{l} C_{4(m-2)+3\_4(m-1)+1} + C_{4(m-2)+4\_4(m-1)+1} \\ + C_{4(m-2)+3\_4(m-1)+2} + C_{4(m-2)+4\_4(m-1)+2} \end{array}\right)}, \quad m = 2, 3, \ldots, N \\ C_{\mathrm{in}2,N} = C_{4(N-1)+3\_4(N-1)+4} + \dfrac{\left(C_{4(N-1)+1\_4(N-1)+3} + C_{4(N-1)+2\_4(N-1)+3}\right) \cdot \left(C_{4(N-1)+1\_4(N-1)+4} + C_{4(N-1)+2\_4(N-1)+4}\right)}{\left(C_{4(N-1)+1\_4(N-1)+3} + C_{4(N-1)+1\_4(N-1)+4} + C_{4(N-1)+2\_4(N-1)+3} + C_{4(N-1)+2\_4(N-1)+4}\right)} \end{cases} \quad (19)$$

$$C_{M,m} = \frac{\left(C_{4(m-1)+2\_4(m-1)+4} \cdot C_{4(m-1)+1\_4(m-1)+3} - C_{4(m-1)+1\_4(m-1)+4} \cdot C_{4(m-1)+2\_4(m-1)+3}\right)}{\left(C_{4(m-1)+1\_4(m-1)+3} + C_{4(m-1)+1\_4(m-1)+4} + C_{4(m-1)+2\_4(m-1)+3} + C_{4(m-1)+2\_4(m-1)+4}\right)} \quad (20)$$

$$\begin{cases} r_{Lf,m} = \omega_0 L_{f,m}/Q, & r_{L1,m} = \omega_0 L_{1,m}/Q,\ r_{L2,m} = \omega_0 L_{2,m}/Q \\ r_{C1,m} = 1/\left(\omega_0 (C_{1,m} - C_{M,m}) Q\right), & r_{C2,m} = 1/\left(\omega_0 (C_{2,m} - C_{M,m}) Q\right) \\ r_{CM,m} = 1/(\omega_0 C_{M,m} Q), & r_{Cf,m} = 1/(\omega_0 C_{f,m} Q),\ Y_{CM,m} = 1/\left(j\omega_0 C_{M,m}\right) \\ Y_{Lf,m} = 1/\left(j\omega_0 L_{f,m} + r_{Lf,m}\right), & Y_{L1,m} = 1/\left(j\omega_0 L_{1,m} + r_{L1,m}\right),\ Y_{RL,m} = 1/R_{L,m} \\ Y_{L2,m} = 1/\left(j\omega_0 L_{2,m} + r_{L2,m}\right), & Y_{C1,m} = 1/\left(1/j\omega_0 (C_{1,m} - C_{M,m}) + r_{C1,m}\right) \\ Y_{C2,m} = 1/\left(1/j\omega_0 (C_{2,m} - C_{M,m}) + r_{C2,m}\right), & Y_{Cf,m} = 1/\left(j\omega_0 C_{f,m} + r_{Cf,m}\right) \end{cases} \quad (21)$$

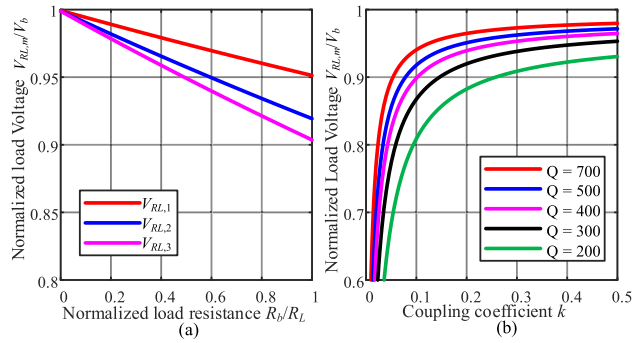

Fig. 11. Voltage analysis. (a) Normalized load voltage variations versus the normalized load resistance ($k = 0.15$ and $Q = 500$). (b) Load voltage variations with different coupling coefficients and quality factors ($N = 3$ and $R_b/R_L = 0.6$).

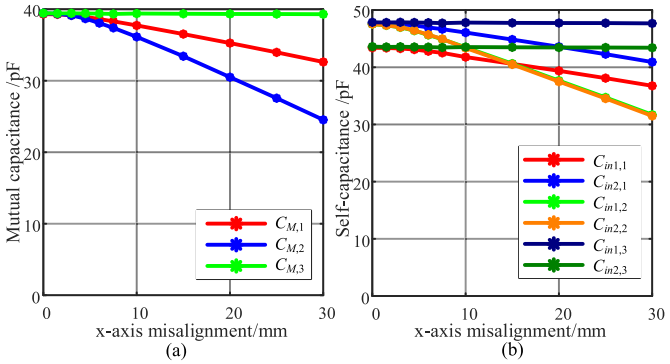

Fig. 12. X-axis misalignment. (a) Mutual capacitance variations. (b) Self-capacitances variations.

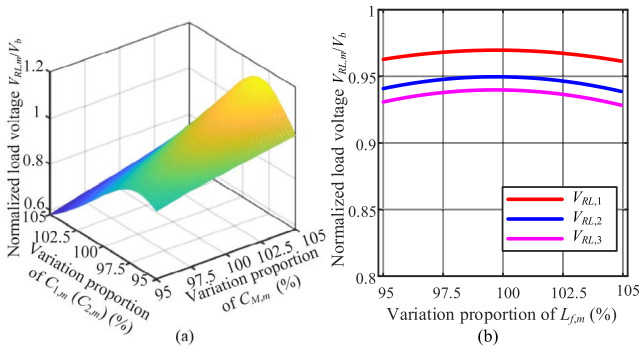

Fig. 13. Output voltage versus (a) variation proportion of $C_{1,m}$ ($C_{2,m}$) and $C_{M,m}$ with the fixed $L_{f,m}$ and (b) variation proportion of $L_{f,m}$ with the fixed repeater coupler ($Q = 500$ and $N = 3$).

are within around 6% when the x-axis misalignment changes by 5%. Fig. 13(a) elaborates the output voltage variation versus the variation of the self-capacitance $C_{1,m}$ ($C_{2,m}$) and mutual capacitance $C_{M,m}$ with the fixed $L_{f,m}$ when the quality factor Q is 500 and the number of loads N is 3. It can be observed that the normalized load voltage changes from 0.6 to 1.2 when $C_{M,m}$ and $C_{1,m}$ ($C_{2,m}$) varied by ±5%. Thus, it is essential to ensure the fixation of the capacitive repeater coupler. It can be concluded that the proposed system is apt to the scenario with small or even no misalignment such as powering online monitoring systems, miner light charging cabinets [13], or reefer containers [20]. Fig. 13(b) illustrates the output voltage variation versus the variation of the compensation inductance $L_{f,m}$ with the fixed repeater coupler in the experiment when the quality factor Q is 500 and the number of loads N is 3. It can be observed that with an increasing $L_{f,m}$, the output voltage decreases. Moreover, the load voltage drop is slightly bigger if it is farther from transmitting unit 0. This is an inherent problem in the CPT system because of the high operating frequency. Besides, when the compensation inductance $L_{f,m}$ varied by ±5%, as shown in Fig. 13(b), the output voltage variation is within 2%, which is acceptable in practical applications to guarantee the performance.

B. System Efficiency

All currents flowing through the system can be calculated as

$$\begin{cases} \boldsymbol{I}_{Lf,\ \mathrm{m}} = \left(\boldsymbol{V}_{P(4(m-2)+4)} - \boldsymbol{V}_{P(4(m-1)+1)}\right) \cdot Y_{Lf,m}, \\ \qquad \boldsymbol{I}_{C1,m} = \boldsymbol{V}_{P(4(m-1)+2)} \cdot Y_{C1,m} \\ \boldsymbol{I}_{L1,m} = \left(\boldsymbol{V}_{P(4(m-1)+1)} - \boldsymbol{V}_{P(4(m-1)+2)}\right) \cdot Y_{L1,m}, \\ \qquad \boldsymbol{I}_{C2,m} = \boldsymbol{V}_{P(4(m-1)+3)} \cdot Y_{C2,m} \\ \boldsymbol{I}_{L2,m} = \left(\boldsymbol{V}_{P(4(m-1)+3)} - \boldsymbol{V}_{P(4(m-1)+4)}\right) \cdot Y_{L2,m} \\ \boldsymbol{I}_{Cf,m} = \boldsymbol{V}_{P(4(m-1)+1)} \cdot Y_{Cf,m}, \\ \qquad \boldsymbol{I}_{RL,m} = \boldsymbol{V}_{P(4(m-1)+4)} \cdot Y_{RL,m}. \end{cases} \tag{25}$$

The efficiency η_N for N multiple loads can be derived by dividing the sum of the load output power $P_{o,m}$ ($m = 1, 2, \ldots, N$) by the sum of the input power $P_{\mathrm{in},m}$ ($m = 1, 2, \ldots, N$) in each transmitter–receiver pair, which can be calculated as (26), as shown at the bottom of the next page, where the load output voltages and all currents flowing through the system can be obtained by solving (22)–(25). The parasitic resistances are related to the quality factor, as shown in (21). Thus, the formula for system efficiency is a complex high-order function of the unit number N, the load resistance

$$\mathbf{G}_m = \begin{bmatrix} Y_{Lf,m} + Y_{Cf,m} + Y_{L1,m} & -Y_{L1,m} & 0 & 0 \\ -Y_{L1,m} & Y_{L1,m} + Y_{C1,m} + Y_{CM,m} & -Y_{CM,m} & 0 \\ 0 & -Y_{CM,m} & Y_{L2,m} + Y_{C2,m} + Y_{CM,m} & -Y_{L2,m} \\ 0 & 0 & -Y_{L2,m} & \begin{cases} Y_{L2,m} + Y_{Lf,m} + Y_{RL,m} \\ \quad (m = 1, 2, \ldots, N-1) \\ Y_{L2,m} + Y_{RL,m} \\ \quad (m = N) \end{cases} \end{bmatrix} \tag{23}$$

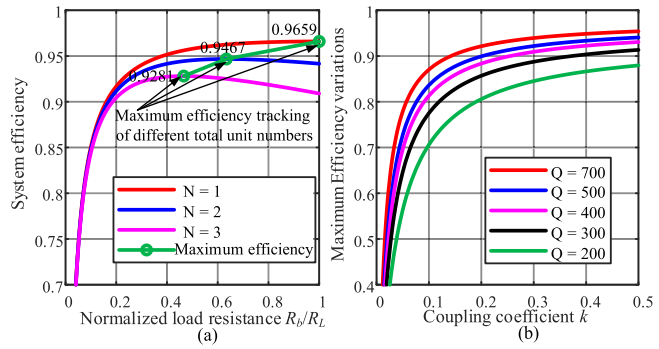

Fig. 14. Efficiency analysis. (a) System efficiency variation against the normalized load resistance ($N = 3$, $k = 0.15$, and $Q = 500$). (b) Maximum achievable efficiency variations with different coupling coefficient k and quality factor Q ($N = 3$, $R_b/R_L = 0.15$).

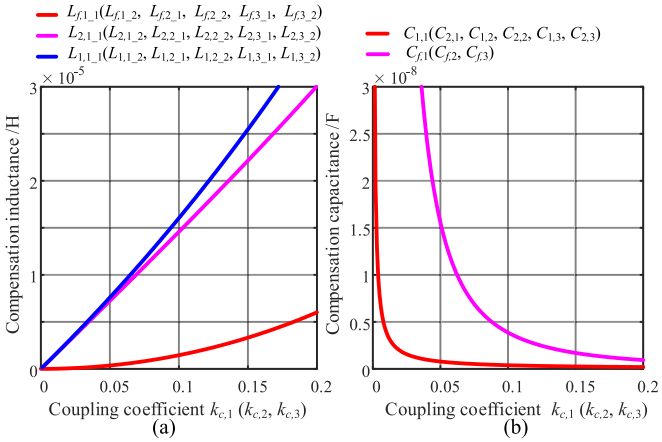

Fig. 15. Parameters of compensation network. (a) Compensation inductances. (b) Compensation capacitances.

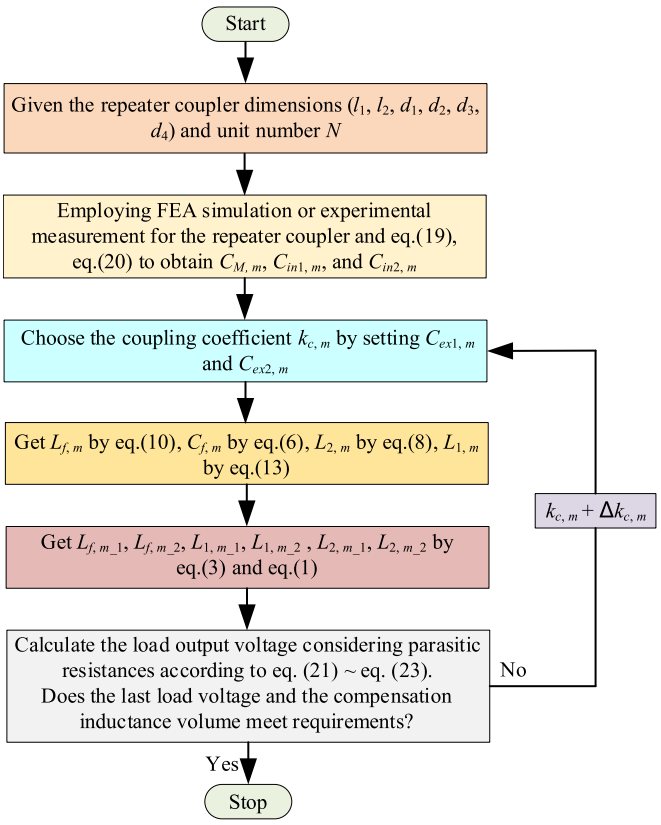

Fig. 16. Design flowchart of the proposed system to tradeoff the minimum load voltage attenuation and the size of the compensation inductances.

$R_{L,m}$, the quality factor Q, and the coupling coefficient $k_{c,m}$ and load voltage $V_{RL,m}$.

The system efficiency variation against the normalized load resistance is shown in Fig. 14(a). It can be seen that there is an optimal load resistance point corresponding to the maximum efficiency, and the optimal normalized load resistance to achieve maximum system efficiency decreases as the repeater number increases. Besides, the system efficiency is restricted by the maximum load number. With the increase of unit number N, the maximum achievable system efficiency declines. This characteristic can be used to indicate the maximum number of repeater units with the required maximum efficiency. In addition, the maximum achievable efficiency is relevant to the coupling coefficient k and quality factor Q, as shown in Fig. 14(b). It can be seen that the higher coupling coefficient and higher quality factor can achieve higher efficiency. It is worth mentioning that, the above conclusions are also tenable when the combination of load resistances is different.

V. Experiments

A. Experimental Prototype

Since this article focuses on the proposed system topology verification, the resistors are utilized to simplify the proposed scheme verification. Four SiC MOSFETs are adopted in the inverter and the switching frequency is 1.5 MHz. The dc voltage of the inverter is 35 V. The repeater coupler dimensions are the same as listed in Table I of Section III; in this case, the mutual capacitance $C_{M,1} = C_{M,2} = C_{M,3} = 39$ pF. As indicated in Section II, with the coupling coefficients determined beforehand, other compensation parameters can be obtained. Fig. 15 shows the parameters of compensation inductors and capacitors with different coupling coefficients.

$$\begin{aligned}\eta_N &= \left(\sum_{m=1}^{N} P_{o,m}\right)\Big/\left(\sum_{m=1}^{N} P_{in,m}\right)\\ &= \frac{\sum_{m=1}^{N}\left(\left|\boldsymbol{V}_{RL,m}\right|^2/R_{L,m}\right)}{\sum_{m=1}^{N}\left(\begin{array}{l}\left|\boldsymbol{I}_{Lf,m}\right|^2 r_{Lf,m} + \left|\boldsymbol{I}_{Cf,m}\right|^2 r_{Cf,m} + \left|\boldsymbol{I}_{L1,m}\right|^2 r_{L1,m} + \left|\boldsymbol{I}_{C1,m}\right|^2 r_{C1,m}\\ + \left|\boldsymbol{I}_{CM,m}\right|^2 r_{CM,m} + \left|\boldsymbol{I}_{C2,m}\right|^2 r_{C2,m} + \left|\boldsymbol{I}_{L2,m}\right|^2 r_{L2,m} + \left|\boldsymbol{V}_{RL,m}\right|^2/R_{L,m}\end{array}\right)}\\ &= = f\left(N, R_{L,m}, Q, k_{c,m}\right)\end{aligned} \tag{26}$$

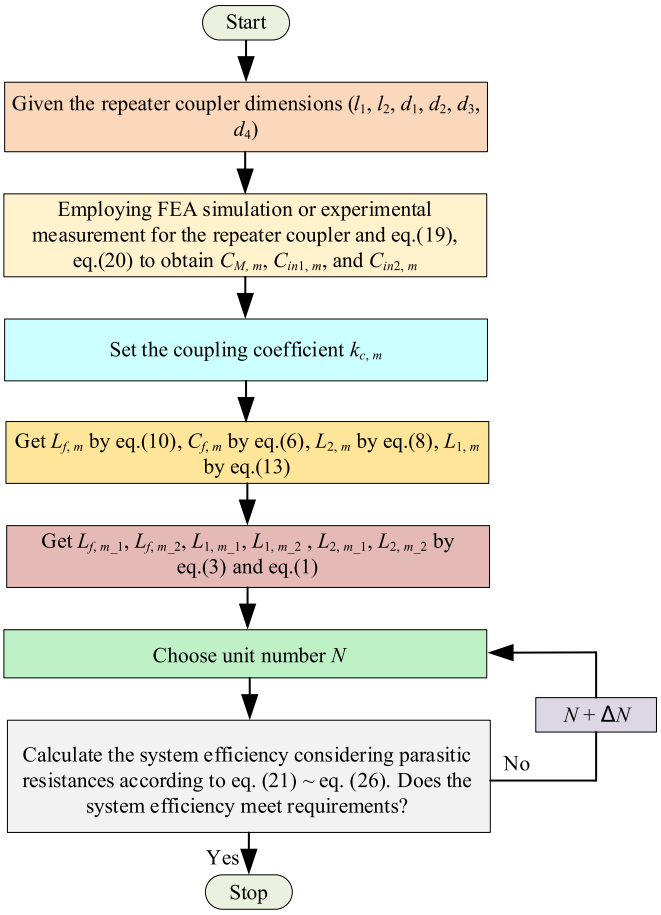

Fig. 17. Design flowchart of the proposed system to find the optimum value of the unit number N with the required optimum efficiency.

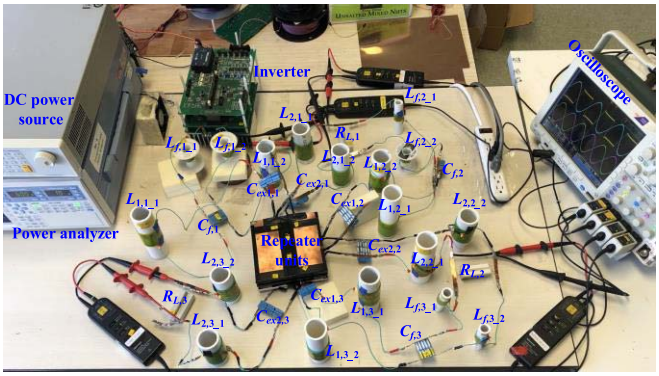

Fig. 18. Experimental setup with three loads.

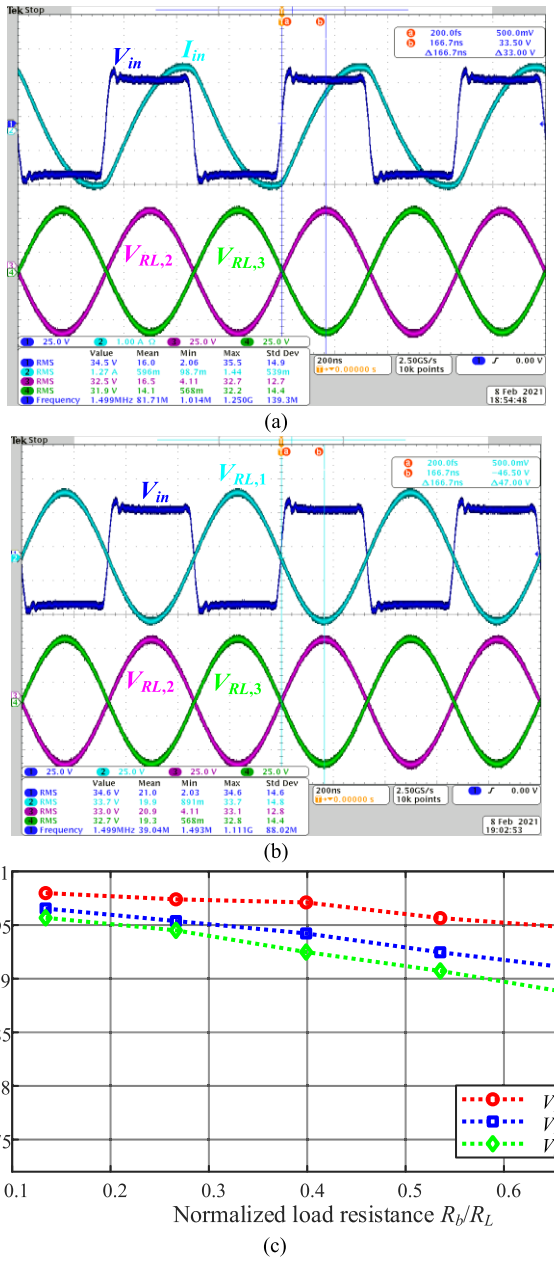

Fig. 19. Experimental results. (a) Experimental waveforms of inverter output voltage, current, and second and third load output voltages ($R_b/R_L = 0.399$). (b) Experimental waveforms of inverter output voltage and all load output voltages ($R_b/R_L = 0.27$). (c) Load voltage variation against the increasing normalized load resistances.

With the increasing coupling coefficient, the compensation inductances increase and the compensation capacitances decrease. As indicated in Section IV, a higher coupling coefficient and higher quality factor are beneficial for achieving a smaller load voltage attenuation and a larger maximum efficiency in the proposed system. If the required normalized voltage of the last load is larger than 0.8, the coupling coefficient should be larger than about 0.08 when the quality factor is 500 and the unit number is 3, as shown in Fig. 11(b). A shown in Fig. 15, a larger coupling coefficient will result in larger compensation inductances, which contributes to a larger system volume. Considering the tradeoff between the minimum load voltage attenuation and the size of the compensation inductances, the coupling coefficient is chosen as 0.15. In this case, the compensation network parameters are listed in Table II. The design flowchart of the proposed system to tradeoff the minimum load voltage attenuation and the size of the compensation inductances is shown in Fig. 16. It is worth noting that even if there are tolerances in different repeater plates, the compensation inductances and the compensation capacitances can be designed separately for the corresponding transmitter–receiver pair to obtain the same load output voltages. It means the design of the proposed system does not require all the repeater units to be exactly identical to obtain the same load output voltages. Once the repeater

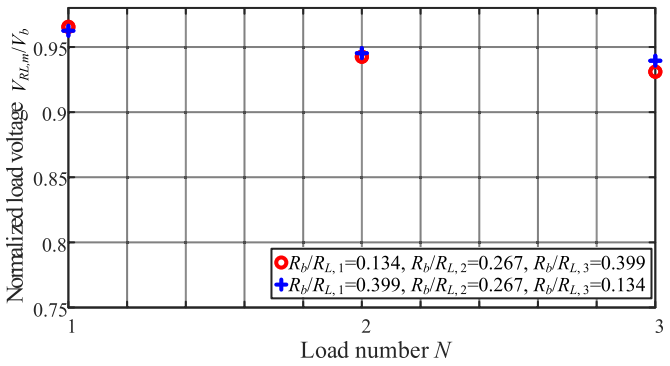

Fig. 20. Load voltage variations with different normalized load resistances.

coupler is determined beforehand, it will not change. Then, the compensation circuit parameters of each fixed repeater unit can be obtained according to the calculation process in Section II to ensure unchanged output voltages.

If the coupling coefficient is fixed beforehand, the proposed system design process to find the optimum value of the unit number N with the required optimum efficiency is shown in Fig. 17. When the required maximum system efficiency is larger than 92%, the maximum unit number N is 3 in accordance with Fig. 14(a). Different applications focus on different performances. In scenarios where the area of the installed capacitive coupler is limited, the voltage drop is the main performance worth considering. In a long-distance transmission application, the system efficiency is a key factor to be considered. Considering the above design procedure, a prototype with three loads is setup, as shown in Fig. 18, to verify the proposed system. Meanwhile, it should be noted that the prerequisite of obtaining the parameters is to ensure the CV outputs and input ZPA. In practical applications, the strict input ZPA will increase the switching noises of the inverter, which induces system efficiency decrease and electro-magnetic interference increase. The solution is to make the input current I_{in} lag inverter output voltage V_{in} to facilitate zero-voltage switching (ZVS) of the MOSFETs in the inverter [22]. Thus, $L_{1,1\_1}$ and $L_{1,1\_2}$ slightly decrease at the same time to achieve ZVS. The compensation inductors are made by 660-strand Litz wires on a hollow plastic tube to reduce the conduction losses arising from the skin effect. Film capacitors from KEMET are adopted as compensation capacitors.

B. Experimental Results

Fig. 19(a) shows that the inverter output current I_{in} lags the inverter output voltage V_{in}, which indicates ZVS is achieved, thereby the switching noises can be greatly eliminated. The experiment waveforms of the inverter output voltage and the three-load output voltages are shown in Fig. 19(b). As evident, the first load output voltage $V_{RL,1}$ and the third load output voltage $V_{RL,3}$ are 180 out of phase with the inverter output voltage V_{in}. The second load output voltage $V_{RL,2}$ is in phase with V_{in}. This phenomenon is consistent with the expression in (9). The voltage drop of the load farther from the inverter will be slightly larger. This phenomenon can also be seen in Fig. 19(c). The third load voltage drops to approximately 0.88, which is due to the influence of parasitic resistances

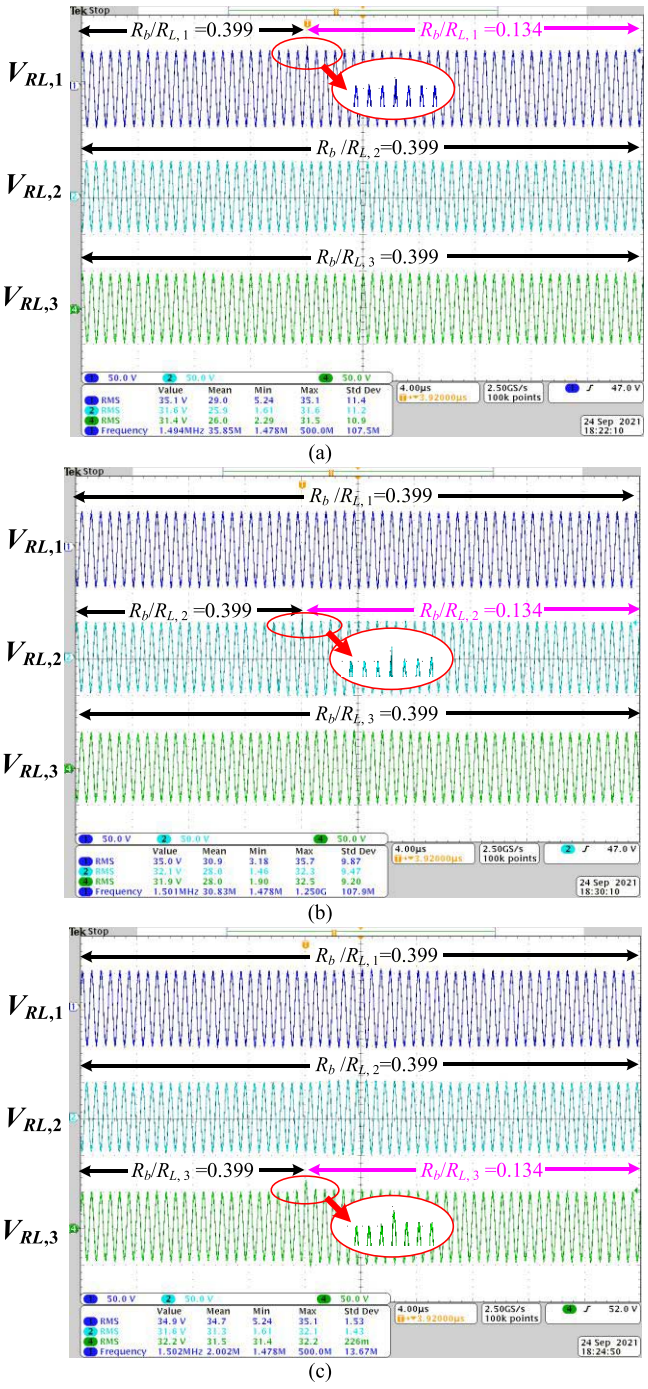

Fig. 21. Experimental results for transient behavior when the normalized load power changes from 0.399 to 0.134. (a) $R_b/R_{L,1}$ changes and the other two loads remain unchanged. (b) $R_b/R_{L,2}$ changes and the other two loads remain unchanged. (c) $R_b/R_{L,3}$ changes and the other two loads remain unchanged.

in the system. The output voltage deviation can be further reduced with a larger k and Q, as shown in the analysis of Section IV-B. It is worth noting that the system can still be regarded as multiple CV outputs although the slight load output voltage attenuation. A dc–dc converter can be employed before each real load to generate a stable output voltage no matter how many loads are powered simultaneously. The main contribution and novelty of this article are that the load power can be almost decoupled, which greatly reduces the interaction

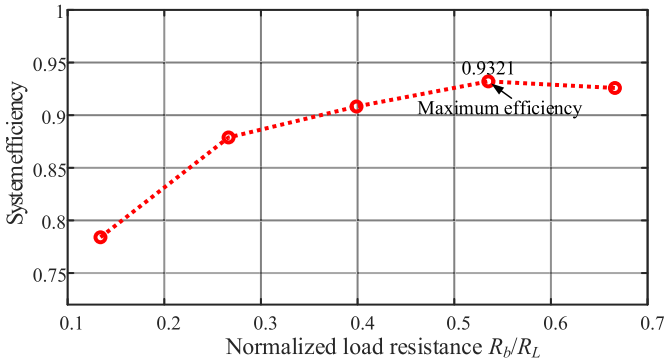

Fig. 22. System efficiency variation against increasing normalized load resistances.

among loads. Therefore, the proposed system can be easily modified to feed the loads with identical voltages. The load voltage variations with different load resistances are shown in Fig. 20. It can be seen that the load voltage variations are kept within 5% with different load resistances. Thus, it is evident that the output voltage of each load output voltage is independent of others.

In order to further verify the decoupled output CV characteristics, initially, all normalized load resistance is 0.399 with the three normalized load output voltages $V_{RL,1}/V_b$, $V_{RL,2}/V_b$, and $V_{RL,3}/V_b$ are around 0.97, 0.94, and 0.92, respectively. Then, the normalized load resistance $R_b/R_{L,1}$, $R_b/R_{L,2}$, and $R_b/R_{L,3}$ suddenly changes to 0.134, respectively; the corresponding output voltages are shown in Fig. 21(a)–(c), respectively. It can be observed that a small voltage spike appears at the starting instant of the load variation and the output voltages will quickly stabilize. The spike in the third load change is a little larger than that in the second load change which is a little larger than that in the first load change. This is because the load voltage variation becomes larger when the further the load is from the first load. The above transient waveforms show that the proposed system renders superior decoupled output CV performance.

The system efficiency against the increasing load resistances is shown in Fig. 22. There is an optimal normalized load resistance to achieve maximum efficiency, which is consistent with the theoretical analysis. The maximum efficiency is around 0.9321 when the normalized load resistance is 0.54. The system efficiency can be further increased with a larger k and Q, as stated in Section IV-B. According to (5), (9), and (26), the system power is proportional to the input voltage V_{in1} and the coupling coefficient $k_{c,m}$. Thus, a high-power level can be achieved by increasing the input voltage with a larger repeater coupler area and smaller external capacitances. Considering the large number of external inductors that are required in the proposed system, in the future, the system operating frequency can be improved and the printed circuit board (PCB)-based inductors can be adopted to increase the power density.

VI. Conclusion

In this article, a power-repeater multiload CPT system has been proposed. A novel repeater design where the transmitting plates are placed perpendicularly to the receiving plates is proposed to eliminate electric coupling with the help of the split-inductors. The whole capacitance model of the capacitive coupler is given and an *L-LCL* compensation network is designed for each capacitive repeater unit to achieve a load-independent constant output voltage. Analytical models are established, which show that a higher quality factor and coupling coefficient can achieve minimum voltage attenuation and maximum efficiency. Experimental results of a three-load setup have validated the effectiveness of the proposed power-repeater multiload CPT system with a maximum efficiency of 93.2%.

References

[1] Z. Zhang, H. Pang, A. Georgiadis, and C. Cecati, "Wireless power transfer—An overview," *IEEE Trans. Ind. Electron.*, vol. 66, no. 2, pp. 1044–1058, Feb. 2019.

[2] V.-B. Vu, V.-T. Phan, M. Dahidah, and V. Pickert, "Multiple output inductive charger for electric vehicles," *IEEE Trans. Power Electron.*, vol. 34, no. 8, pp. 7350–7368, Aug. 2018.

[3] M. Liu, M. Fu, Y. Wang, and C. Ma, "Battery cell equalization via megahertz multiple-receiver wireless power transfer," *IEEE Trans. Power Electron.*, vol. 33, no. 5, pp. 4135–4144, May 2014.

[4] Y. Li *et al.*, "Analysis, design, and experimental verification of a mixed high-order compensations-based WPT system with constant current outputs for driving multistring LEDs," *IEEE Trans. Ind. Electron.*, vol. 67, no. 1, pp. 203–213, Jan. 2020.

[5] H. Yang *et al.*, "Efficiency analysis and optimization method of power-relay IPT systems for reefer containers," *IEEE Trans. Power Electron.*, vol. 36, no. 5, pp. 4942–4947, May 2021.

[6] C. Zhang, D. Lin, N. Tang, and S. Y. R. Hui, "A novel electric insulation string structure with high-voltage insulation and wireless power transfer capabilities," *IEEE Trans. Power Electron.*, vol. 33, no. 1, pp. 87–96, Jan. 2018.

[7] C. Cheng *et al.*, "Load-independent wireless power transfer system for multiple loads over a long distance," *IEEE Trans. Power Electron.*, vol. 34, no. 9, pp. 9279–9288, Sep. 2019.

[8] S. Y. R. Hui, W. Zhong, and C. K. Lee, "A critical review of recent progress in mid-range wireless power transfer," *IEEE Trans. Power Electron.*, vol. 29, no. 9, pp. 4500–4511, Sep. 2014.

[9] F. Lu *et al.*, "A high-efficiency and long-distance power-relay system with equal power distribution," *IEEE J. Emerg. Sel. Topics Power Electron.*, vol. 8, no. 2, pp. 1419–1427, Jun. 2020.

[10] X. Xie, C. Xie, and L. Li, "Wireless power transfer to multiple loads over a long distance with load-independent constant-current or constant-voltage output," *IEEE Trans. Transport. Electrific.*, vol. 6, no. 3, pp. 935–947, Sep. 2020.

[11] C. Cheng, W. Li, Z. Zhou, Z. Deng, and C. Mi, "A load-independent wireless power transfer system with multiple constant voltage outputs," *IEEE Trans. Power Electron.*, vol. 35, no. 4, pp. 3328–3331, Apr. 2020.

[12] V. Vu *et al.*, "A multi-output capacitive charger for electric vehicles," in *Proc. IEEE 26th Int. Symp. Ind. Electron. (ISIE)*, Jun. 2017, pp. 565–569.

[13] W. Zhou, Q. Gao, L. He, B. Luo, R. Mai, and Z. He, "Design of CPT system with multiple constant output voltage pickups using inverse hybrid parameters of capacitive coupler," *IEEE Trans. Ind. Appl.*, vol. 58, no. 1, pp. 1061–1070, Jan. 2022, doi: 10.1109/TIA.2021.3109172.

[14] Y. Chen, Z. Kou, Y. Zhang, Z. He, R. Mai, and G. Cao, "Hybrid topology with configurable charge current and charge voltage output-based WPT charger for massive electric bicycles," *IEEE J. Emerg. Sel. Topics Power Electron.*, vol. 6, no. 3, pp. 1581–1594, Sep. 2018.

[15] Y. Su, S. Xie, A. P. Hu, C. S. Tang, W. Zhou, and L. Huang, "Capacitive power transfer system with a mixed-resonant topology for constant-current multiple-pickup applications," *IEEE Trans. Power Electron.*, vol. 32, no. 11, pp. 8778–8786, Nov. 2017.

[16] M. B. Lillholm, Y. Dou, X. Chen, and Z. Zhang, "Analysis and design of 10-MHz capacitive power transfer with multiple independent outputs for low-power portable devices," *IEEE J. Emerg. Sel. Topics Power Electron.*, vol. 10, no. 1, pp. 149–159, Feb. 2022.

[17] A. Kumar, S. Pervaiz, C.-K. Chang, S. Korhummel, Z. Popovic, and K. K. Afridi, "Investigation of power transfer density enhancement in large air-gap capacitive wireless power transfer systems," in *Proc. IEEE Wireless Power Transf. Conf. (WPTC)*, May 2015, pp. 1–4.

[18] H. Zhang, F. Lu, H. Hofmann, W. Liu, and C. C. Mi, "An LC-compensated electric field repeater for long-distance capacitive power transfer," *IEEE Trans. Ind. Appl.*, vol. 53, no. 5, pp. 4914–4922, Sep./Oct. 2017.
[19] T. Chen, C. Cheng, H. Cheng, C. Wang, and C. Mi, "A multi-load capacitive power relay system with load-independent constant current outputs," *IEEE Trans. Power Electron.*, vol. 37, no. 5, pp. 6144–6155, May 2022.
[20] W. Liu *et al.*, "A multi-load capacitive power transfer system with load-independent characteristic for reefer container application," *IEEE Trans. Power Electron.*, vol. 37, no. 5, pp. 6194–6205, May 2022.
[21] H. Zhang, F. Lu, H. Hofmann, W. Liu, and C. Mi, "A 4-plate compact capacitive coupler design and LCL-compensated topology for capacitive power transfer in electric vehicle charging applications," *IEEE Trans. Power Electron.*, vol. 31, no. 12, pp. 8541–8851, Dec. 2016.
[22] M. Wu *et al.*, "A dual-sided control strategy based on mode switching for efficiency optimization in wireless power transfer system," *IEEE Trans. Power Electron.*, vol. 36, no. 8, pp. 8835–8848, Aug. 2021.

Ting Chen received the B.S., M.S., and Ph.D. degrees from the China University of Mining and Technology, Beijing, China, in 2015, 2017, and 2022, respectively.

From November 2019 to November 2021, she was a Joint Ph.D. Student with the Department of Electrical and Computer Engineering, San Diego State University, San Diego, CA, USA, funded by the China Scholarship Council. Her current research interests include wireless power transfer technologies and power electronic converters.

Chenwen Cheng received the B.S. and Ph.D. degree from Zhejiang University, Hangzhou, China, in 2012 and 2017, respectively, all in electrical engineering.

From 2018 to 2021, he was a Post-Doctoral Researcher with San Diego State University, San Diego, CA, USA. He is currently with Southeast University, Nanjing, China. His research interests include the motor control, renewable power generation, and wireless power transfer technologies.

Hong Cheng received the B.S. degree in electrical engineering from Beihang University, Beijing, China, in 1988, and the Ph.D. degree in electrical engineering from the China University of Mining and Technology, Beijing, in 1993.

She is currently a Professor of power electronics with the School of Mechanical Electronic and Information Engineering, China University of Mining and Technology. Her current research interests include high-power multilevel converters, modeling and control of switching converters, and fault diagnosis of power electronics equipment.

Cong Wang was born in Beijing, China, in 1955. He received the B.S. degree in electrical engineering from Taiyuan University of Technology, Taiyuan, China, in 1982, and the M.S. and Ph.D. degrees in electrical engineering from the China University of Mining and Technology, Beijing, in 1984 and 2005, respectively.

From 1990 to 1991, he was a Visiting Scholar with the University of Bristol, Bristol, U.K. From 2002 to 2003, he was a Senior Visiting Scholar and a Visiting Professor with The University of Tennessee, Knoxville, TN, USA. He is currently a Professor of power electronics with the School of Mechanical Electronic and Information Engineering, China University of Mining and Technology. His current research interests include high-power multilevel converters, high-frequency soft-switching converters, and power electronics in smart grid.

Chunting Chris Mi (Fellow, IEEE) received the B.S.E.E. and M.S.E.E. degrees in electrical engineering from Northwestern Polytechnical University, Xi'an, China, in 1985 and 1988, respectively, and the Ph.D. degree in electrical engineering from the University of Toronto, Toronto, ON, Canada, in 2001.

He is currently a Distinguished Professor and the Chair of the Department of Electrical and Computer Engineering and the Director of the Department of Energy (DOE)-funded Graduate Automotive Technology Education (GATE) Center for Electric Drive Transportation, San Diego State University (SDSU), San Diego, CA, USA. Prior to joining SDSU, he was with the University of Michigan, Dearborn, MI, USA, from 2001 to 2015. His research interests include electric drives, power electronics, electric machines, electrical and hybrid vehicles, wireless power transfer, and power electronics.

Dr. Mi is a fellow of the Society of Automotive Engineers (SAE). He was a recipient of the IEEE Power Electronics Society (PELS) Emerging Technology Award in 2019, the IEEE TRANSACTIONS ON POWER ELECTRONICS Best Paper Award, and two IEEE TRANSACTIONS ON POWER ELECTRONICS Prize Letter awards. He was a recipient of the Albert W. Johnson Lecture Award, which is the highest distinction for any SDSU faculty.